

# Tensor network algorithm by coarse-graining tensor renormalization on finite periodic lattices

Hui-Hai Zhao<sup>1,2,\*</sup>, Zhi-Yuan Xie<sup>3,4</sup>, Tao Xiang<sup>3,5,†</sup> and Masatoshi Imada<sup>1‡</sup>

<sup>1</sup>*Department of Applied Physics, University of Tokyo, Hongo, Bunkyo-ku, Tokyo 113-8656, Japan*

<sup>2</sup>*Institute for Solid State Physics, University of Tokyo, Kashiwanoha, Kashiwa, Chiba 277-8581, Japan*

<sup>3</sup>*Institute of Physics, Chinese Academy of Sciences, P.O. Box 603, Beijing 100190, China*

<sup>4</sup>*Department of Physics, Renmin University of China, Beijing 100872, China and*

<sup>5</sup>*Collaborative Innovation Center of Quantum Matter, Beijing 100190, China*

(Dated: October 13, 2015)

We develop coarse-graining tensor renormalization group algorithms to compute physical properties of two-dimensional lattice models on finite periodic lattices. Two different coarse-graining strategies, one based on the tensor renormalization group and the other based on the higher-order tensor renormalization group, are introduced. In order to optimize the tensor-network model globally, a sweeping scheme is proposed to account for the renormalization effect from the environment tensors under the framework of second renormalization group. We demonstrate the algorithms by the classical Ising model on the square lattice and the Kitaev model on the honeycomb lattice, and show that the finite-size algorithms achieve substantially more accurate results than the corresponding infinite-size ones.

## I. INTRODUCTION

Tensor network algorithms, which have been widely developed recently<sup>1–13</sup>, provide efficient and promising numerical tools for studying two and higher dimensional classical statistical and quantum lattice models. For a classical statistical model<sup>5,14–16</sup> or a lattice gauge model<sup>17,18</sup>, the partition function can be expressed as a tensor network state, and physical quantities can be obtained by contracting this tensor network state. In the quantum case, the tensor network state provides a faithful representation of the ground state wave function. For example, the ground state of Affleck-Kennedy-Lieb-Tasaki model<sup>19</sup>, which is the so-called valence-bond-solid state, can be rigorously represented as a tensor network state.

A tensor-network wave function was first used in the numerical calculation of the Heisenberg model on the honeycomb lattice by Niggemann *et al* in 1997<sup>1</sup>. Later on, Sierra *et al* proposed a more general ansatz on the tensor network states<sup>20</sup>. By utilizing tensor network state as a variational wave function, Nishino *et al* proposed a method to calculate three-dimensional Ising model<sup>2</sup>. In 2004, Verstraete and Cirac argued that a natural generalization of the matrix product state to two and higher dimensions is a projected entangled pair state (PEPS)<sup>3</sup>, and showed that this kind of states satisfies automatically the area law of entanglement entropy. As a generalization of the PEPS, the projected entangled simplex state (PESS)<sup>12</sup> was proposed by Xie *et al* to account for the entanglement effect of all particles in a simplex. This simplex entanglement effect is important in the study of frustrated quantum lattice systems. By introducing disentanglers to the tensor network to reduce the short range entanglement, the multi-scale entanglement renormalization ansatz<sup>4</sup> can provide logarithmic correction to the area law of entanglement entropy<sup>21</sup> in one-dimensional critical systems. Tensor network al-

gorithms have not only shown prominent success in the study of both classical statistical and quantum lattice models, but also drawn intense interests in the study of quantum field theory<sup>23,24</sup>, interacting fermions<sup>25–28</sup>, and disordered systems<sup>29</sup>.

During the past years, several algorithms have been developed to contract two-dimensional infinite lattice tensor network states. These algorithms can be divided into two categories. The first is to represent a tensor-network state as a product of transfer matrix along a spatial direction, and reduce the problem of evaluating the trace of the tensor-network state to a problem of finding the dominant eigenvalues of the transfer matrix. To diagonalize the transfer matrix, a number of approaches can be used. One is the transfer-matrix renormalization group<sup>30–32</sup> as well as its generalization such as the corner-transfer-matrix renormalization group<sup>33–36</sup>, the other is the infinite time-evolving block decimation based on the evolution of matrix product state<sup>6,37,38</sup>.

The second is to contract the tensor network state by taking a coarse graining tensor renormalization. This includes the method of tensor renormalization group (TRG)<sup>5,39</sup> method proposed by Levin and Nave based on the singular value decomposition (SVD) of local tensors. The TRG is a local optimization approach, which optimizes the truncation error only locally. A global optimization approach of TRG, developed by Xie *et al*.<sup>9,16</sup>, was proposed to take into account for the second renormalization effect of the environment tensors. This method is called the second renormalization group (SRG) and can significantly reduce the truncation error in comparison with the TRG. In 2012, a different coarse-graining scheme based on the higher-order singular value decomposition (HOSVD), which is now referred as HOTRG<sup>11,22</sup>, was proposed. Similarly to the TRG, the HOTRG is a local optimization method. The corresponding global optimization method is called higher-order second renormalization group (HOSRG)<sup>11</sup>.

The above coarse graining TRG methods allow us to evaluate thermodynamic quantities directly in the thermodynamic limit, without invoking finite-size scaling. However, the truncation error is accumulated at each coarse-graining step. The accuracy of the method is reduced with the increase of the lattice size, especially in a system close to a critical point where the correlation length diverges. The error can be reduced by increasing the bond dimension  $D$  of local tensors retained in the truncation. Furthermore, a finite  $D$  scaling analysis can be performed to extrapolate to the infinite  $D$  limit.<sup>40</sup>

The PEPS algorithm was first introduced by Verstraete and Cirac to study finite lattice systems in 2004<sup>3</sup>, and was further improved by a number of groups<sup>42,43,45–48</sup>. It works more efficiently in a system with open boundary conditions than in a system with periodic boundary conditions, due to the heavy computational cost in the evaluation of a double-layer tensor network state in a periodic system. The coarse graining TRG or SRG can be applied to a finite periodic system<sup>27,49</sup>. But a systematic study on this kind of methods is still not available.

In this paper, we explore the finite-lattice SRG algorithm in a periodic boundary system. We propose a sweeping scheme to evaluate the environment tensor using the SRG. It is found that the sweeping can greatly improve the accuracy of the SRG, especially in the case the truncation error is large. As for the Kitaev model considered in this work, we find that the SRG with sweeping can significantly reduce the truncation error comparing to that of the TRG. It suggests that the SRG can be used to determine very accurately the renormalization effect of the environment in a finite lattice system by sweeping. This, together with the finite-size scaling analysis of the finite-lattice results, gives a powerful numerical tool for studying lattice models in two or higher dimensions.

This paper is arranged as follows. In order to make the paper as self-contained as possible, we first briefly review the TRG, SRG and other related methods introduced in Refs. 3, 5, 9, 11, and 16. In Sec. II, the construction of tensor network from classical statistical models and quantum lattice models are described. In Sec. III, the TRG and HOTRG methods are briefly reviewed. In Sec. IV, as an example, the implementation of the SRG on the honeycomb lattice, and the HOSRG on the square lattice are illustrated. In Sec. V, the application of SRG and HOSRG on finite lattices are explained. In Sec. VI, we benchmark our algorithms for the classical Ising model on the square lattice and the Kitaev model on the honeycomb lattice. Finally, we summarize in Sec. VII.

## II. TENSOR NETWORK STATE

As elaborated in Ref. 16, the partition function of any classical statistical lattice model with short-range interactions can be represented as a tensor network state. A simple example is the two-dimensional Ising model, de-

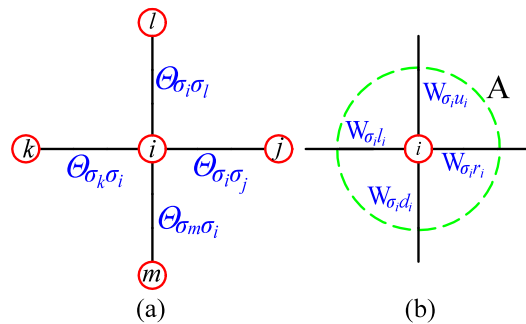


Figure 1. (color online) (a) Pictorial representation of the partition function defined by Eq. (2), where  $\Theta_{\sigma_i \sigma_j}$ ,  $\Theta_{\sigma_k \sigma_i}, \dots$  are the Boltzmann weights associated with neighboring sites. (b) Every Boltzmann weight is decomposed as in Eq. (3), and a site tensor  $A$  is constructed from 4  $W$  matrices associated with the same site as in Eq. (5).

finied by the Hamiltonian

$$H = - \sum_{\langle i,j \rangle} \sigma_i \sigma_j, \quad (1)$$

where  $\sigma_i = \pm 1$  is the Ising variable at site  $i$ . The partition function of this model is given by

$$Z = \sum_{\{\sigma\}} \prod_{\langle i,j \rangle} \exp(\beta \sigma_i \sigma_j), \quad (2)$$

where  $\sum$  is to sum over all spin configurations  $\{\sigma\}$ , and  $\beta$  is the inversed temperature. The Boltzmann weight associated with site  $i$  and  $j$  (Fig. 1(a)) can be decomposed as<sup>11</sup>

$$\Theta_{\sigma_i \sigma_j} = e^{\beta \sigma_i \sigma_j} = \sum_{u_i} W_{\sigma_i u_i} W_{\sigma_j u_i}. \quad (3)$$

Here,  $W$  is  $2 \times 2$  matrix, defined by

$$W = \begin{pmatrix} \sqrt{\cosh \beta} & \sqrt{\sinh \beta} \\ \sqrt{\cosh \beta} & -\sqrt{\sinh \beta} \end{pmatrix}, \quad (4)$$

where  $u_i$  is the index representing the bond basis state between sites  $i$  and  $j$ . On square lattice, A local tensor at site  $i$  can then be constructed as

$$A_{u_i d_i l_i r_i}^i = \sum_{\sigma_i} W_{\sigma_i u_i} W_{\sigma_i d_i} W_{\sigma_i l_i} W_{\sigma_i r_i}, \quad (5)$$

where  $u_i, d_i, l_i$  and  $r_i$  represents the bonds between the  $i$  site and its up, down, left and right nearest neighbor sites, respectively. A graphical representation of this equation is shown in Fig. 1(b).

By substituting the above equations to Eq. (2), it is straightforward to show that the partition function of the Ising model on a square lattice can be expressed as a product of local tensors(Fig. 1)<sup>16</sup>

$$Z = \text{Tr} \prod_i A_{u_i d_i l_i r_i}^i, \quad (6)$$

where  $i$  runs over all the lattice sites and the trace is to sum over all bond indices.

For a quantum lattice model, the ground state wave function can also be expressed as a tensor network state. Both PEPS and PESS belong to this type of wave functions. Let us take a square-lattice PEPS functions<sup>3</sup> as an example:

$$|\Psi\rangle = \sum_{\{m\}} \text{Tr} \prod_i a_{u_i d_i l_i r_i}^i [m_i] |m_1 m_2 \dots m_N\rangle, \quad (7)$$

where  $i$  runs over all the lattice sites. The trace is to sum over all bond indices. The dimension of each bond index is assumed to be  $D$ . The difference between the PEPS wave function in Eq. (7) and the tensor network representation of the partition function in Eq. (6) is that Eq. (7) contains extra indices  $m_1 m_2 \dots m_N$  which represent physical degrees of freedom on all lattice sites.

The PEPS is a variational wave function for the ground state. Unlike the tensor network states for classical statistical models, the tensor elements of PEPS are unknown. The PEPS can be determined by variationally minimizing the ground state energy. But the computational cost for doing this is very high. A more efficient approach for determining the PEPS is to take an imaginary time evolution by applying the projection operator  $\exp(-\tau H)$  successively to a random PEPS, where  $\tau$  is a small parameter. For a Hamiltonian, which contains only nearest neighbor interactions

$$H = \sum_{\langle i,j \rangle} h_{ij}, \quad (8)$$

the imaginary time evolution generally starts by taking the Suzuki-Trotter decomposition to divide approximately the evolution operator into a sequence of local two-site operators

$$e^{-\tau H} = \prod_{\langle i,j \rangle} e^{-\tau h_{ij}} + O(\tau^2). \quad (9)$$

The imaginary time evolution is then implemented by applying these two-site projection operators to the PEPS successively.

To do the projection, let us first do the following singular value decomposition for the two-site projection operator

$$\langle m_i m_j | e^{-\tau h_{ij}} | n_i n_j \rangle = \sum_k U_{m_i n_i, k} S_k V_{m_j n_j, k}, \quad (10)$$

where  $U$  and  $V$  are unitary matrices of dimension  $d^2$  with  $d$  the dimension of local physical basis space.  $S$  is a semi-positive diagonal matrix, and its diagonal elements are the singular values of the projection operator. By applying the projection operator  $\exp(-\tau h_{ij})$  to the PEPS, the local tensors at sites  $i$  and  $j$  change to

$$\tilde{a}_{udl(xk)}^i [m] = \sum_n a_{udlx}^i [n] U_{mn, k} \sqrt{S_k}, \quad (11)$$

$$\tilde{a}_{ud(xk)r}^j [m] = \sum_n a_{udxr}^j [n] V_{mn, k} \sqrt{S_k}. \quad (12)$$

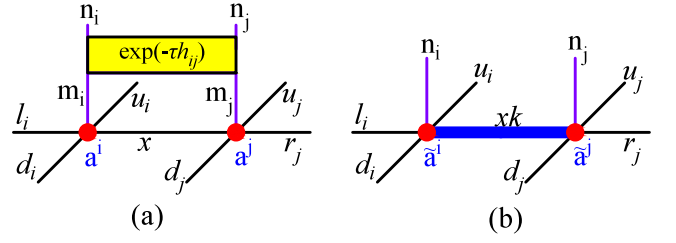


Figure 2. (color online) (a) Pictorial representation of applying the operator  $\exp(-\tau h_{ij})$  on the associated neighboring site tensors  $a^i$  and  $a^j$ . (b) Site tensors  $\tilde{a}^i$  and  $\tilde{a}^j$  after the evolution by Eq. (11) and (12), where the dimension of thicker blue bond is increased.

The bond dimension on the link connecting  $i$  and  $j$  are enlarged by a factor of  $d^2$ . A graphical representation of these equations is shown in Fig. 2.

To continue the imaginary time evolution, the bond dimension on the link between  $i$  and  $j$  needs to be truncated. The truncated local tensors,  $\tilde{a}^i$  and  $\tilde{a}^j$ , can be determined by minimizing the following difference between the tensors before and after the truncation<sup>3</sup>

$$f(a) = \left| |\Psi\rangle - |\tilde{\Psi}\rangle \right|^2, \quad (13)$$

where  $|\tilde{\Psi}\rangle$  and  $|\Psi\rangle$  are the PEPS wave functions before and after truncations, respectively.  $f(a)$  is a quadratic function of  $a^i$  and  $a^j$ . It can be generally expressed as<sup>42</sup>

$$f(a) = a^\dagger \mathcal{N} a - 2a^\dagger b + \text{const}, \quad (14)$$

where  $a$  represents  $a^i$  or  $a^j$ .  $\mathcal{N}$  is obtained from the norm  $\langle \Psi | \Psi \rangle$  by removing  $a^\dagger$  in  $\langle \Psi |$  and  $a$  in  $|\Psi\rangle$ , and  $b$  is obtained from  $\langle \Psi | \tilde{\Psi} \rangle$  by removing  $a^\dagger$  in  $\langle \Psi |$ .

To explicitly show how  $\mathcal{N}$  and  $b$  are derived from the PEPS wave function, let us first define the following double tensors

$$A_{\mu\mu'} = \sum_m a_{udlr}^* [m] a_{u'd'l'r'} [m], \quad (15)$$

$$\tilde{A}_{\mu\mu'} = \sum_m \tilde{a}_{udlr}^* [m] a_{u'd'l'r'} [m], \quad (16)$$

where  $\mu$  and  $\mu'$  are the simplified notations of bond indices  $udlr$  and  $u'd'l'r'$ , respectively. Then,  $\mathcal{N}$  and  $b$  tensor networks corresponding to site  $i$  can be expressed as

$$\mathcal{N}_{\mu_i m_i, \mu'_i m'_i}^i = \delta_{m_i, m'_i} \text{Tr} \prod_{q \neq i} A_{\mu_q \mu'_q}^q, \quad (17)$$

$$b_{\mu_i m_i}^i = \text{Tr} \tilde{a}_{\mu'_i}^i [m_i] \tilde{A}_{\mu_j \mu'_j}^j \prod_{q \neq i, j} A_{\mu_q \mu'_q}^q, \quad (18)$$

where  $\text{Tr}$  is to contract all connecting bond indices.

$\langle \Psi | \Psi \rangle$  and  $\langle \Psi | \tilde{\Psi} \rangle$  are called closed tensor networks since they are composed of closed bonds, and the contraction of the closed tensor network comes out to be a scalar.

$\mathcal{N}$  and  $b$  are called open tensor networks since they are composed of open bonds in addition to the closed bonds, and the contraction of an open tensor network comes out to be a tensor, which is usually called the environment tensor. In Eq. (14),  $\mathcal{N}$  is the environment tensor of  $a^\dagger$  and  $a$ , and  $b$  is the environment tensor of  $a^\dagger$ .

By minimizing the functional  $f(a)$ , one can update the local tensors. This procedure is called full-update<sup>3,42</sup>. An entanglement mean-field approach can also be used to update the local tensors without contracting all tensors<sup>7</sup>. This can avoid the contraction of the full double tensor network, which requires demanding computation time. Nevertheless, this kind of contraction is still needed in the evaluation of expectation value

$$\langle \mathcal{O} \rangle = \frac{\langle \Psi | \mathcal{O} | \Psi \rangle}{\langle \Psi | \Psi \rangle}. \quad (19)$$

### III. COARSE GRAINING TENSOR RENORMALIZATION

The previous section describes the construction of the tensor network. Then, the following task is to perform the network contraction, which can be achieved by coarse-graining tensor renormalization. The general idea of these methods is to reduce number of tensors by a coarse-graining renormalization procedure iteratively until the tensor network becomes small enough to be exactly contracted. Levin and Nave<sup>5</sup> proposed the TRG to study two-dimensional classical models based on the SVD of local tensors. Later, Xie et al<sup>11</sup> proposed the HOTRG to study two and three dimensional lattice models based on the HOSVD of local tensors. Both of these two methods optimize the truncation error only locally, which do not consider the contribution from environment lattice sites. We briefly reiterate the procedures of TRG and HOTRG in this section.

#### A. Tensor renormalization group

We here take a two-sublattice honeycomb-lattice tensor network as an example to describe the TRG method. The TRG method on the square lattice is described in Appendix A.

There are two steps at each coarse-graining procedure. The first step is to rewire a honeycomb lattice to a triangle-honeycomb lattice as shown in Fig. 3(a). This is done by contracting a pair of neighboring-site tensors on two sides of a dashed line, which is explicitly described as

$$M_{jn,km} = \sum_z A_{zjk}^i B_{zmn}^i. \quad (20)$$

and as shown pictorially in Fig. 3(b). Then the SVD is applied to decompose  $M$  in the perpendicular direction

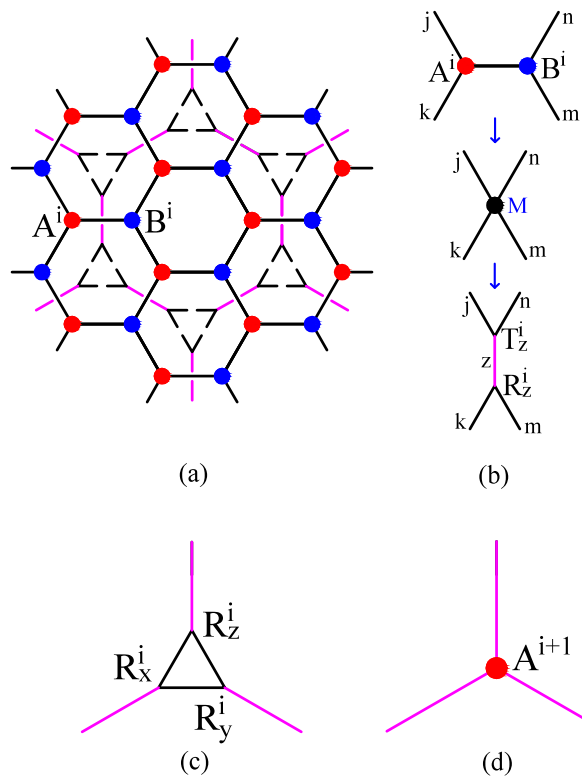


Figure 3. (color online) TRG coarse-graining scheme for honeycomb-lattice tensor network<sup>5</sup>. Two sublattice tensor network is assumed. (a) Rewire a honeycomb lattice to a triangle-honeycomb lattice. (b) Schematic representation of Eq 20 and 21. (c) Three  $i$ -th scale tensors are coarse grained to one  $(i+1)$ -th scale tensor  $A^{i+1}$  as in (d).

and keep  $\chi$  largest singular values

$$M_{jn,km} \approx \sum_{z=1}^{\chi} U_{jn,z} \Lambda_z V_{km,z}, \quad (21)$$

where truncation is performed and  $\chi$  largest singular values are kept. To estimate the quality of the truncation, we define the truncation error as

$$\varepsilon = 1 - \frac{\sum_{z=1}^{\chi} \Lambda_z^2}{\sum_z \Lambda_z^2}. \quad (22)$$

Then, the construction of  $R_z^i$  and  $T_z^i$  as shown pictorially in the bottom of Fig. 3(b) can be done as

$$R_z^i = U \Lambda^{\frac{1}{2}}, \quad T_z^i = V \Lambda^{\frac{1}{2}} \quad (23)$$

The second step is to contract three tensors on every triangle in the rewired lattice to form a honeycomb-lattice tensor network of which the size is reduced by a factor of 3 (see Fig. 3(c) to (d)). By repeating this coarse-graining procedure, one can finally obtain a network with six tensors on a hexagon which can be contracted exactly. The contraction of the whole tensor network can then be achieved.

The computational cost for the TRG on the honeycomb lattices scales as  $O(\chi^6)$ , because the most time consuming computation is to apply SVD on  $\chi^2 \times \chi^2$  matrices.

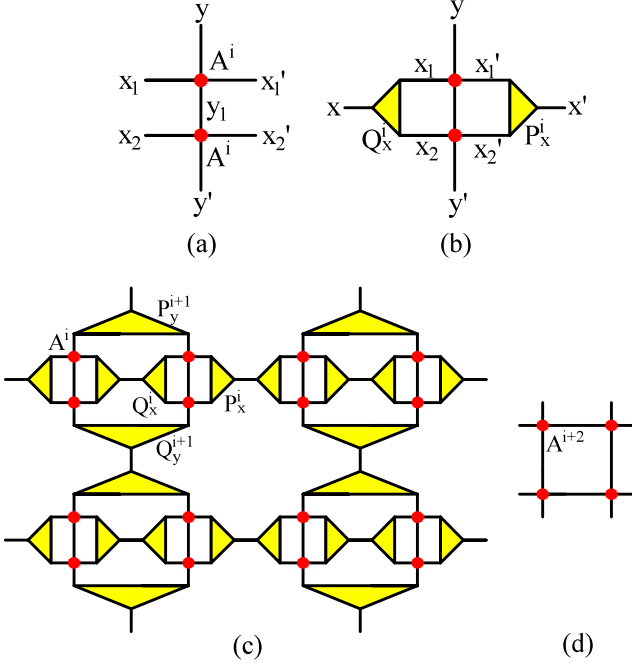


Figure 4. (color online) HOTRG coarse-graining scheme for square-lattice tensor network<sup>11</sup>. (a) two tensors aligned vertically are contracted. (b) Construct projector  $P_x^i$  and  $Q_x^i$  illustrated by (yellow) triangles by HOSVD. (c) One vertical and one horizontal coarse graining steps are performed, and four  $i$ -th scale tensors  $A^i$  are coarse grained to one  $(i+2)$ -th scale tensor  $A^{i+2}$  shown in (d).

## B. Higher-order tensor renormalization group

We next summarize the HOTRG procedure<sup>11</sup>. During the TRG procedure, the lattice shape changes alternately every after the scale renormalization from the  $i$ -th to  $i+1$ -th scale, while HOTRG keeps lattice shape during the procedure. For simplicity, we take a single-sublattice square-lattice tensor network as an example to illustrate the HOTRG method. At every coarse graining step, we contract 2 tensors to form one higher scale tensor (Fig. 4(b)), on which 2 projectors  $P_x^i$  and  $Q_x^i$  are applied to make the truncation of the bond dimension. Here we explain how to construct  $P_x^i$  and  $Q_x^i$ . As shown in Fig. 4(a), two tensors aligned vertically are contracted

$$M_{(x_1 x_2)(x'_1 x'_2)yy'}^i = \sum_{y_1} A_{x_1 x'_1 y_1 y_1}^i A_{x_2 x'_2 y_1 y_1}^i. \quad (24)$$

In order to make the truncation, we apply the HOSVD

on  $M^i$  as<sup>11</sup>

$$M_{(x_1 x_2)(x'_1 x'_2)yy'}^i = \sum_{ijkl} S_{ijkl} U_{(x_1 x_2)i}^L U_{(x'_1 x'_2)j}^R U_{y^k}^U U_{y^l}^D, \quad (25)$$

where the sub-tensors in the core tensor  $S$  are reordered so that the order satisfies their Frobenius norm as

$$n < n', \quad \text{if } |S_{\dots n \dots}| \geq |S_{\dots n' \dots}|, \quad (26)$$

where  $n$  and  $n'$  belong to the same index.

Then, we can make truncation by comparing

$$\varepsilon_L = \sum_{i > \chi} |S_{i, \dots, \dots}|^2 \quad (27)$$

and

$$\varepsilon_R = \sum_{j > \chi} |S_{\dots, j, \dots}|^2. \quad (28)$$

if  $\varepsilon_L < \varepsilon_R$ , we keep the first  $\chi$  columns in  $U^L$  to form the truncated matrix  $\tilde{U}^L$ , thereby the projectors in the horizontal direction can be constructed as

$$P_x^i = \tilde{U}^L, \quad Q_x^i = (\tilde{U}^L)^\dagger. \quad (29)$$

If  $\varepsilon_L \geq \varepsilon_R$ , the way of constructing the projectors follows Eq. (29) by replacing  $\tilde{U}^L$  with  $\tilde{U}^R$  which is obtained from the truncation of  $U^R$ .

After we obtain the projectors, we can contract 2 site tensors with corresponding projectors to form a renormalized tensor network of which the size is reduced by a factor of 2, and we can coarse grain the lattice alternately along the horizontal and vertical directions as shown in Fig. 3(c)(d). The computational cost for this tensor contraction scales as  $O(\chi^7)$ , which is the leading cost for HOTRG on the square lattice.

Up to now, we have discussed the general procedure of TRG and HOTRG algorithms to contract the tensor network. We note here that the partition function and the expectation values of the physical observables can be evaluated naturally in these coarse-graining procedure. To be concrete, let us take HOTRG as an example. Suppose  $\lambda_i$  is the renormalization coefficient extracted (in order to keep the amplitude of any tensor element within the digit allowed in computers) in the  $i$ -th iteration from a single local tensor  $T_i$ . For example,  $\lambda_i$  may be defined as the element of  $T_i$  with the largest absolute value before renormalizing the amplitudes of the element of  $T_i$ . Then, the partition function can be expressed as

$$\begin{aligned} Z &= \text{Tr} \left\{ \prod_{i=1}^N T_0 \right\} \\ &= \text{Tr} \left\{ \prod_{i=1}^{N/2} T_1 \right\} \cdot \lambda_1^{N/2} \\ &= \dots \\ &= \text{Tr} \{ T_\nu \} \cdot \lambda_1^{N/2} \lambda_2^{N/2^2} \dots \lambda_\nu^{N/2^\nu}. \end{aligned} \quad (30)$$

Here  $N$  is the total number of tensors. If the system is reduced to a single tensor  $T_\nu$  after  $\nu$  steps, then  $N = 2^\nu$ . Actually this is the effective formula we used in the practical calculation:

$$\frac{\ln Z}{N} = \sum_{i=1}^{\nu} \frac{1}{2^i} \ln \lambda_i + \frac{\ln(\text{Tr}\{T_\nu\})}{2^\nu}. \quad (31)$$

For simplicity, a single sub-lattice structure is assumed. It seems that the free energy is determined only by the coefficients  $\lambda_i$ s and the final tensor  $T_\nu$ . In practical computations, in most cases,  $\nu = 40$  or so is sufficient to make the free energy reach the asymptotic value expected in the thermodynamic limit. Similarly one can also calculate the expectation value of any physical quantities. For a local operator  $\hat{O}$ , its expectation value can be expressed as

$$\begin{aligned} \langle \hat{O} \rangle &= \frac{\text{Tr}\{\hat{O}e^{-\beta H}\}}{\text{Tr}\{e^{-\beta H}\}} \\ &= \frac{\text{Tr}\{S_0 \prod_{i=1}^{N-1} T_0\}}{\text{Tr}\{\prod_{i=1}^N T_0\}} \\ &= \frac{\text{Tr}\{S_1 \prod_{i=1}^{N/2-1} T_1\}}{\text{Tr}\{\prod_{i=1}^{N/2} T_1\}} \\ &= \dots \\ &= \frac{\text{Tr}\{S_n\}}{\text{Tr}\{T_n\}} \end{aligned} \quad (32)$$

where  $S_0$  is a local tensor which contains the information of operator and usually dubbed as an *impurity* tensor. The denominator and numerator are nothing but tensor networks, with the only difference that the numerator has an impurity tensor. The central idea is to see how the impurity tensor evolves in the coarse-graining process. After the contraction as in the evaluation of the partition function, one can finally get the ratio. By employing the same renormalization coefficients  $\lambda_i$ s in each iteration for the two networks (one for the denominator and the other for the numerator), we obtain a practical formula to calculate the expectation value of a single operator as in Eq.(32) after cancellation of  $\lambda_i$ s.

For two-body operators such as spin-spin correlation function, or other complicated operators, the methods are quite similar, where the only difference is the number of impurity tensors in the numerator.

#### IV. SECOND RENORMALIZATION

TRG and HOTRG are local optimization methods which optimize the approximation of the local targeted system without any considerations of the environment. In order to optimize the approximation of the whole tensor network, it is necessary to consider the effect of environment tensor network with respect to the tensors needed to be truncated. At the same time, it is also

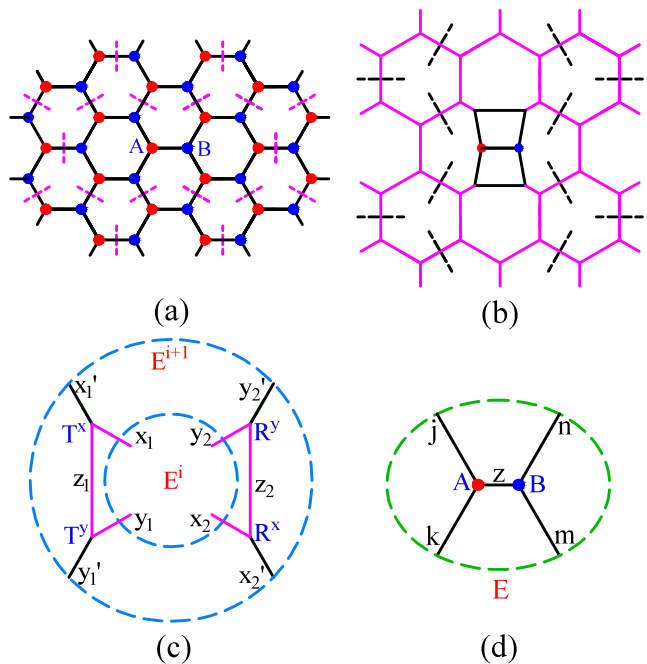


Figure 5. (color online) SRG procedure for honeycomb lattice<sup>9,16</sup>. From (a) to (b) is one coarse-graining step for environment sites. A pair of neighboring site tensors on two sides of a dashed line are contracted and then decomposed along the dashed line. (c) Relation between the neighboring scales environments  $E^i$  and  $E^{i+1}$  (dashed circles) as represented in Eq. (33). (d) Environment tensor  $E$  with system site tensors  $A$  and  $B$ .

necessary to calculate the environment tensor during the imaginary time evolution. Therefore, we have developed SRG<sup>9,16</sup> and HOSRG<sup>11</sup> methods to consider the renormalization effect of the environment and optimize the approximation in the contraction of whole tensor networks. For the convenience of describing finite size coarse-graining methods in the next section, we reiterate the key procedures of SRG and HOSRG here.

#### A. Second renormalization group

The general idea of SRG is to find an effective representation of the environment by coarse graining the surrounding environment tensor network with respect to the target tensors, and then use the information of the environment to do global optimization in the approximation of the target tensors. To be specific, let us explain how to implement the SRG on the honeycomb lattice here. The SRG method on the square lattice is described in Appendix B.

Figure 5 shows the SRG procedure for the honeycomb lattice<sup>9,16</sup>. First, we do forward iteration by the TRG, in order to contract the whole surrounding tensor network. In this iteration, the local tensors at each scale is stored. A general guiding clue here is that one should

make the targeted system as compact as possible in the coarse-graining process. As in Fig. 5, we keep a pair of two neighboring sites unchanged, and coarse grain the environment tensor network as shown in Figs. 5(a) and (b) by the TRG. Since we assume that the environment is always infinite at every coarse-graining step of the system sites, we need to apply the coarse graining in the environment for a sufficient number of steps until converged.

Second, we do backward iteration from the closing scale in order to find effective environment of the targeted system, represented also as a local tensor. In this iteration, the central problem is to find the recursion relation between the environment of two neighboring scales. Figure 5(c) schematically shows the relation between the environments of the neighboring scales, which can be represented by the following iteration formula<sup>16</sup>

$$E_{x_1 y_1 x_2 y_2}^i = E_{x'_1 y'_1 x'_2 y'_2}^{i+1} T_{z_1 x_1 x'_1}^x T_{z_1 y_1 y'_1}^y R_{z_2 x_2 x'_2}^x R_{z_2 y_2 y'_2}^y, \quad (33)$$

where the repeated indices imply summation.

After a forward iteration, we are able to do backward iteration to contract the network by starting from tracing out the outermost bonds and follow Fig. 5(c) to compute the environment tensor from higher to lower scales. Eventually, we can obtain the environment tensor  $E = E^1$  which is defined as the outer part of the green ellipse in Fig. 5(d).

Then, we use the obtained environment tensor to do global optimization of the local tensor (namely, the target tensor). Here the global optimization means that the local truncation is chosen so that, compared to the untruncated case, the difference of the partition function or the summation of the whole tensor network is minimized, as concretely detailed below.

After finding out the environment tensor  $E$  (green dashed ellipse in Fig. 5(d)), we can contract the system sites  $A$  and  $B$  to form a matrix  $M$  as in Eq. 20. The SVD is then applied to decompose  $E$ ,

$$E_{km,jn} = \sum_z X_{km,z} \Omega_z Y_{jn,z}, \quad (34)$$

where  $X$  and  $Y$  are unitary matrices.

Then, we can take the environment contribution into account by constructing the following tensor<sup>16</sup>

$$\tilde{A}_{z_1 z_2} = \sum_{mnjk} \Omega_{z_1}^{\frac{1}{2}} Y_{jn,z_1} M_{jn,km} X_{km,z_2} \Omega_{z_2}^{\frac{1}{2}}. \quad (35)$$

We compute the SVD of  $\tilde{A}$  and make truncation to keep  $\chi$  largest singular values  $\Lambda$ , the corresponding left singular vectors  $U$  and right singular vectors  $V$  as

$$\tilde{A}_{z_1 z_2} \approx \sum_{z=1}^{\chi} U_{z_1 z} \Lambda_z V_{z_2 z}. \quad (36)$$

Finally,  $M_{jn,km}$  in Eq. (20) can be truncated and de-

composed as a product of two tensors

$$M_{jn,km} \approx \sum_{z=1}^{\chi} R_{jnz} T_{kmz}, \quad (37)$$

where

$$R_{jnz} = \sum_{z_1} Y_{jn,z_1} \Omega_{z_1}^{-\frac{1}{2}} U_{z_1 z} \Lambda_z^{\frac{1}{2}} \quad (38)$$

$$T_{kmz} = \sum_{z_2} X_{km,z_2} \Omega_{z_2}^{-\frac{1}{2}} V_{z_2 z} \Lambda_z^{\frac{1}{2}}, \quad (39)$$

are two rank-3 tensors similarly to Eq. (23), which are on two neighboring triangles connected by one bond.

Since the aim of the SRG is to optimize the truncation globally, the truncation error of the SRG can be defined as

$$\varepsilon = 1 - \frac{\sum_{mnjkz} E_{km,jn} R_{jnz} T_{kmz}}{\sum_{mnjk} E_{km,jn} M_{jn,km}}. \quad (40)$$

This definition is consistent with Eq. (22), because if we take  $E = M$ , Eqs. (22) and (40) are equivalent each other.

We can then contract three tensors on every triangle in the rewired lattice to form one rank-3 tensor as a coarse-grained site on a renormalized honeycomb-lattice tensor network as shown from Fig. 3(c) to (d). Then, we can repeat this coarse-graining procedure until the network can be contracted exactly. Thus the contraction of the whole tensor network can be completed.

The computational cost of tensor contraction in backward iteration, which is shown in Fig. 5(c) and Eq. (33), scales as  $O(\chi^6)$ . This is the same complexity as the SVD, so the computational cost for the SRG on the honeycomb lattice is  $O(\chi^6)$ .

One can also apply the TRG to a square lattice directly with the computational cost scaling as  $O(\chi^{10})$ , which is described in Appendix B. Fortunately, there exists a much cheaper method which needs to convert a square lattice to a honeycomb lattice, and this can be done by SVD of every fourth-order site tensor to two third-order tensors along the same diagonal direction (Magenta dashed lines in Fig. 6(a)) as proposed in Ref. 16. After this conversion, we can employ the honeycomb-lattice SRG method to contract this tensor network. Obviously, this kind of conversion can be easily implemented in the infinite-size lattice, because the boundary condition is not important in the infinite system. For a finite square lattice with the PBC, this conversion generates a honeycomb lattice with the hexagonal periodic boundary, which means that the parallel sides of the boundary (green dashed hexagon in Fig. 6(b)) are equivalent sides. The honeycomb lattice with hexagonal periodic boundary can be calculated by TRG/SRG, and the size of lattice that can be handled is  $(2 \times 3^{\frac{L}{2}}) \times (2 \times 3^{\frac{L}{2}})$ , where  $L$  is the number of coarse-graining steps.

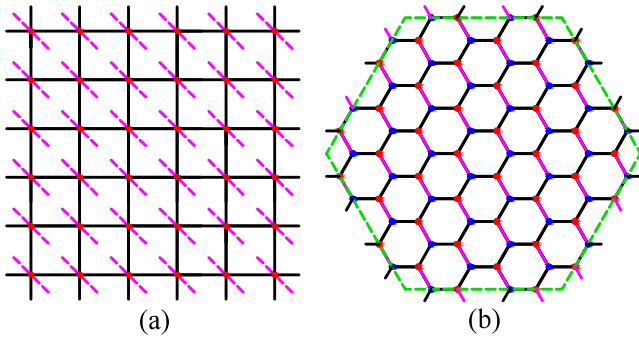


Figure 6. (color online) Conversion from a square lattice to a honeycomb lattice tensor network<sup>16</sup>. (a) Every square lattice site tensor is decomposed by SVD along the direction indicated by dashed (magenta) lines, and the  $6 \times 6$  periodic boundary square lattice is converted to (b) 72 sites honeycomb lattice with periodic boundary indicated by green dashed hexagon. The parallel sides of the boundary are equivalent sides.

### B. Higher-order second renormalization group

The aim of the HOSRG is also to optimize the approximation of the whole tensor network by considering the renormalization effect of the environment. However, instead of the environment of site tensors, the environment of bonds is computed. We keep 2 bonds unchanged, and coarse grain the environment tensor network as shown in Fig. 7(a) and (b) by the HOTRG.

Then, we can employ backward iteration to calculate the environment tensor. Fig. 7(c) schematically shows the relation between the environments of the neighboring scales, which can be represented by the following iteration formula<sup>11</sup>

$$E_{x_1 y_1 x_2 y_2}^i = E_{x'_1 y'_1 x'_2 y'_2}^{i+1} P_{x_2 x_2 x_4}^x Q_{x'_1 x_1 x_3}^x A_{x_3 x_4 y_2 y'_2}^{i+1}. \quad (41)$$

We start contracting the environment network by tracing out the outermost bonds and follow Fig. 7(c) to compute the environment tensor from higher to lower scales. Eventually, we can obtain the bond density matrix  $\rho$  by tracing out all the bonds except the bonds to be truncated, which is denoted as the bonds inside the green ellipse in Fig. 7(d).

$\rho$  is not always a symmetric matrix, so the diagonalization of  $\rho$  may contain negative or complex eigenvalues. Instead, we construct the projectors by a biorthonormal transformation<sup>50</sup>. First, We compute the SVD of  $\rho$  and make truncation to keep  $\chi$  largest singular values  $\Omega$ , the corresponding left singular vectors  $X$  and right singular vectors  $Y$  as

$$\rho_{jk, mn} \approx \sum_x X_{jk, x} \Omega_x Y_{mn, x}. \quad (42)$$

Then, we compute the SVD on  $Y^\dagger X$

$$\sum_{jk} Y_{jk, x_1} X_{jk, x_2} = \sum_x U_{x_1 x} \Lambda_x V_{x_2 x}. \quad (43)$$

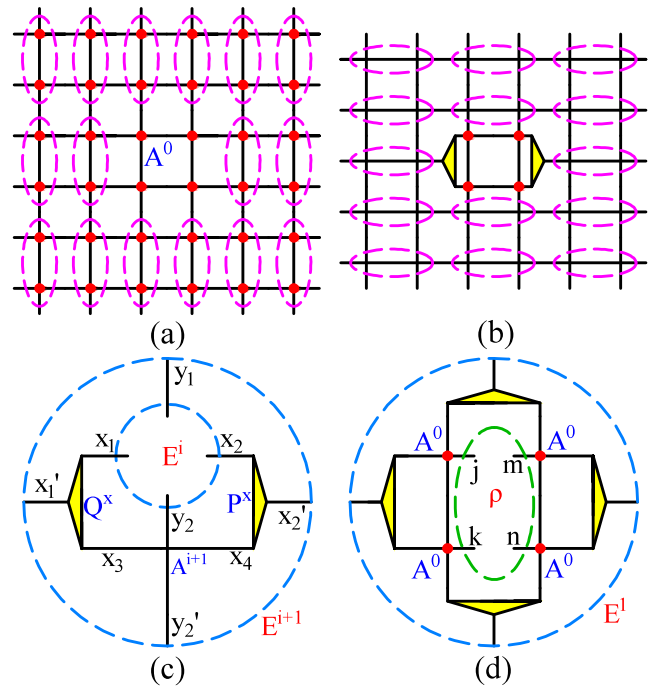


Figure 7. (color online) HOSRG procedure for square lattice<sup>11</sup>. From (a) to (b) is one coarse-graining step for environment sites. 4 site tensors in every dashed circle are coarse grained into 1 tensor. (c) Relation between the neighboring scales environments  $E^i$  and  $E^{i+1}$  (dashed circles) as represented in Eq. (41). (d) Bond density matrix  $\rho$  can be obtained by tracing out all bonds outside the green ellipse.

Finally, we can construct the projectors

$$P_{jk, x}^x = \sum_{x_2} X_{jk, x_2} V_{x_2 x} \Lambda_x^{\frac{1}{2}} \quad (44)$$

$$Q_{mn, x}^x = \sum_{x_1} Y_{mn, x_1} U_{x_1 x} \Lambda_x^{\frac{1}{2}}. \quad (45)$$

The construction of projectors associated with vertical bonds is almost the same, except that we need to compute the bond density matrix of vertical bonds.

The computational cost for tensor contraction in backward iteration, which is shown in Fig. 7(c) and Eq. (41) scales as  $O(\chi^7)$ , while the computational cost for the construction of bond density matrix  $\rho$  scales as  $O(\chi^8)$ , which is shown in Fig. 7(d) Therefore, the leading computational cost for HOSRG on the square lattice is  $O(\chi^8)$ .

## V. ALGORITHM FOR FINITE PERIODIC SYSTEMS

The SRG and HOSRG introduced in IV are for the infinite lattices, since at every coarse-graining step of system sites, the size of environment tensor networks are always assumed to be infinite. In order to contract a finite-lattice

tensor network with the PBC by coarse-graining tensor renormalization methods, we will introduce the implementation of SRG and HOSRG on finite lattices. These finite lattice methods can be also applied to the infinite lattice, since it further improves the accuracy by reducing the accumulation error at every coarse-graining step.

Let us start by considering the finite-size SRG method on the honeycomb lattice with the hexagonal PBC, and assume that the tensor network contains two sublattices  $A^0$  and  $B^0$ . Suppose that the honeycomb tensor network contains  $8 \times 3^L$  sites, where  $L$  is the total number of the coarse-graining steps. The following procedure is employed:

1. The TRG is employed to obtain and store site tensors  $A^i, B^i$  ( $i = 0, \dots, L$ ) and also  $R_\gamma^i, T_\gamma^i$  ( $i = 0, \dots, L-1, \gamma = x, y, z$ ) at every scale.  $R_\gamma^i, T_\gamma^i$  are obtained from the transformation of  $A^i, B^i$  along the  $\gamma$  direction as shown in Fig. 3(b).
2. For the  $i$ -th scale tensor network which contains  $8 \times 3^{L-i}$  sites, we compute the environment of a pair of neighboring sites  $A^i, B^i$  according to Fig. 5. The number of coarse-graining steps required to contract the environment tensor network is  $L-i$ , and  $i, i+1, \dots, L$ -th scale tensors  $(R_\gamma^i, T_\gamma^i), (R_\gamma^{i+1}, T_\gamma^{i+1}), \dots, (R_\gamma^{L-1}, T_\gamma^{L-1})$  and  $(A^L, B^L)$  are needed to calculate the environment tensor  $E$ .
3. After the environment tensor  $E$  is obtained, the environment contribution can be taken into account by Eq. (34) and Eq. (35). Then, we can construct  $R_\gamma^i, T_\gamma^i$  by Eq. (B6) and Eq. (B7), respectively.
4. After all the  $R_\gamma^i, T_\gamma^i$  updated in the same way, we can contract  $R_z^i, R_x^i$  and  $R_y^i$  to form updated  $A^{i+1}$ , and contract  $T_z^i, T_x^i$  and  $T_y^i$  to form updated  $B^{i+1}$  according to Fig. 3(c)(d).
5. Since  $A^{i+1}, B^{i+1}$  has been updated, tensors from  $(i+2)$ -th scale to  $L$ -th scale should be changed accordingly before going to update tensors of  $(i+2)$ -th scale. Here we use the TRG to obtain the  $(i+2)$ -th scale to the  $L$ -th scale tensors which are required for coarse graining from the  $(i+1)$ -th scale to  $(i+2)$ -th scale tensor network.
6. Repeat the steps 2 to 5 from  $i = 0$  to  $i = L-1$ .

The difference from the SRG method for the infinite lattice is that the size of the lattice is fixed and the number of tensors in the environment is reduced in the process of coarse graining. In the original SRG method for the infinite lattice, although the truncation error is reduced by considering the environment contribution, the truncation error at every coarse-graining step will accumulate. This accumulation appears unavoidable for the infinite lattice algorithm. However, the finite-size algorithm has

its own advantage for the possibility of controlling and eliminating the error accumulation. In order to reduce the accumulation error, we employ a sweeping scheme, which is similar as the sweeping in finite size DMRG algorithm. The sweeping scheme is to repeat the step 2 to step 6 until converged. The computational cost for finite SRG scales as  $O(N_s \cdot \chi^6)$ , where  $N_s$  is the number of sweeping and  $\chi^6$  is the cost for SRG calculation.

In the finite size SRG method described above, when the tensors at the  $i$ -th scale are updated by the SRG, all the tensors at higher scales are updated simultaneously because of the step 5. As a matter of fact, if the updating of  $A^{i+1}$  and  $B^{i+1}$  changes the tensors sufficiently slow, we can assume that the environment of  $A^{i+1}$  and  $B^{i+1}$  does not change. Then, we can skip step 5 to reduce the computation cost.

The finite-size HOSRG method is very similar to the finite-size SRG method, so we only explain the difference of them. Let us consider a square lattice with the PBC. Suppose that the tensor network contains  $4 \times 2^L$  sites, where  $L$  is the total number of coarse-graining steps. In the step 1 and step 5, the TRG is replaced by the HOTRG. Since the HOTRG/HOSRG scheme does not contain the lattice rewiring,  $R_\gamma^i, T_\gamma^i$  do not exist. Instead, we need to store all the projectors  $P_\gamma^i, Q_\gamma^i$  ( $i = 0, \dots, L-1, \gamma = x, y$ ).

## VI. RESULTS

### A. Ising model on square lattice

To benchmark our finite-size algorithms, we first calculate the Ising model on the square lattice with the PBC. The partition function can be exactly evaluated on any lattice size<sup>51</sup>. We first convert the square-lattice tensor network to that of the honeycomb lattice as shown in Fig. 6. Then, we apply a finite SRG on the honeycomb lattice to contract the tensor network, so the computational cost scales as  $O(\chi^6)$ . In this calculation, we find that the result is almost unchanged after the sweeping procedure. The reason is that the truncation error of the finite SRG on this model is sufficiently small and the number of the required coarse graining is also small, so that the accumulated error does not practically cause a damage in the final result even without the sweeping thanks to the simplicity of the model.

Figure 8 shows the relative error of the free energy as a function of  $L$  for the Ising model on the  $L \times L$  square lattice at the critical temperature of the infinite lattice,  $T_c = 2/\ln(1 + \sqrt{2})$ . We can see that the relative error basically increases with the increase in the lattice size. This general trend applies to the infinite-size calculation, where the error is the largest if one fixes  $\chi$ . Therefore, by applying the finite-size scaling to obtain infinite-size free energy as shown in Fig. 9, the extrapolated infinite-size result becomes more accurate than that of infinite-size SRG calculation. In the extrapolation, we utilize the

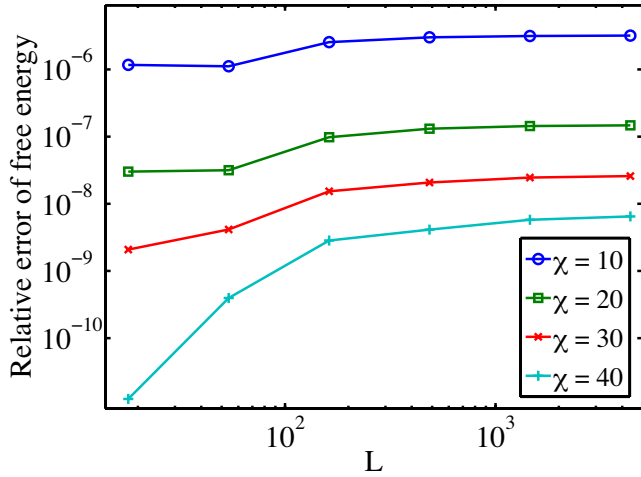


Figure 8. (color online) Relative errors of free energy as a function of  $L$  for  $L \times L$  square-lattice Ising model computed by the SRG method for finite lattices with  $\chi = 10, 20, 30, 40$ . The calculation is at the critical temperature of the infinite lattice, namely at the temperature  $T = T_c = 2/\ln(1 + \sqrt{2})$ . The exact free energy for  $18 \times 18, 54 \times 54, 162 \times 162, 486 \times 486, 1458 \times 1458,$  and  $4374 \times 4374$  are  $-2.114134648928, -2.110149135739, -2.109706474810, -2.109657292382, -2.109651827694,$  and  $-2.109651220507,$  respectively.

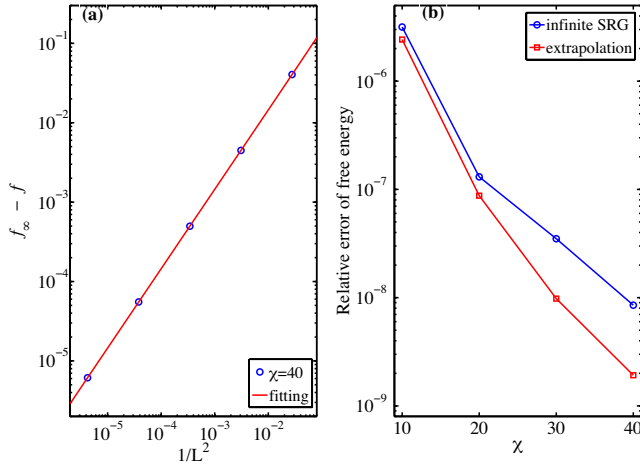


Figure 9. (color online) (a)  $(f_\infty - f(L))$  as a function of  $1/L^2$  (blue circles) at  $T_c = 2/\ln(1 + \sqrt{2})$ , where  $f(L)$  is the free energy. The red line shows the fit to the function  $f_\infty - f(L) = a/L^2 + b/L^4$ . (b) Relative errors of free energy as a function of  $\chi$  computed by infinite SRG (blue line with circles) and by finite SRG with extrapolation to infinite size (red line with squares) by following the procedure in (a).

known finite-size scaling of free energy with respect to  $1/L^2$  at the critical temperature to the second order<sup>41</sup>

$$f_\infty - f(L) = a/L^2 + b/L^4 + O(L^6), \quad (46)$$

where  $f_\infty$  is the extrapolated infinite-size free energy.

We also apply the finite HOSRG method to study the square-lattice Ising model. When the lattice size is sim-

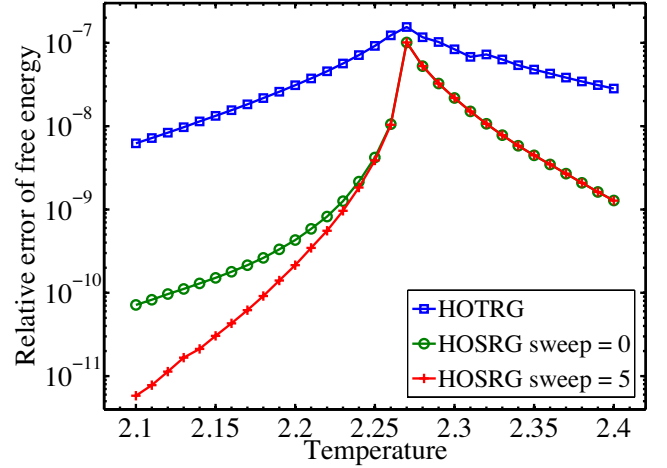


Figure 10. (color online) Relative errors of free energy as a function of temperature for the square-lattice Ising model by the HOTRG (square), the HOSRG at the size  $2^{25} \times 2^{25}$  without (open circle) and with (cross) 5 times sweeping. All the results are obtained with  $\chi = 20$ .

ilar to that in the SRG calculation above, typically, up to  $10^4$  in the linear dimension  $L$ , we also find that the sweeping does not improve the accuracy significantly in this simple model. However, when we increase the number of coarse-graining steps, namely further increase the system size beyond  $L = 10^4$ , the accumulated error becomes more and more significant so that the sweeping provides us with a substantially better accuracy. Figure 10 shows the relative error of the free energy as a function of temperature for the  $2^{25} \times 2^{25}$  square lattice, which can be practically regarded as the infinite lattice. We find that the sweeping scheme improves the accuracy below the critical temperature. Therefore, even when one computes properties in the thermodynamic-limit, our finite coarse-graining methods offers a higher accuracy than the corresponding infinite-lattice methods.

## B. Kitaev model on honeycomb lattice

Next, we calculate the Kitaev model on the honeycomb lattice<sup>52</sup> with an equal amplitude of bond couplings defined by

$$H = \frac{1}{2} \sum_{\langle i,j \rangle_\gamma} \sigma_i^\gamma \sigma_j^\gamma, \quad \gamma = z, x, y, \quad (47)$$

where the Ising anisotropy depends on the three different directions of bonds of the honeycomb lattice. Here,  $\sigma_i^\gamma$  represents the Ising spin at  $i$  site with the Ising anisotropy axis in the  $\gamma$  direction. This model is exactly solvable at any lattice size with any kind of the PBC<sup>52</sup>. The exact ground state is a highly frustrated spin liquid and it is gapless in the thermodynamic limit. The infinite PEPS calculation<sup>53</sup> shows good agreement with the exact

ground state energy in the infinite lattice, although the lattice rotational symmetry is artificially broken due to the mapping from honeycomb lattice to brick-wall lattice.

In our calculation, the wave function is represented as a honeycomb PEPS with the hexagonal shaped PBC, and the imaginary time evolution is employed to determine the ground state. As described in Sec. II, the computation of the environment is needed to optimize tensors during imaginary time evolution. We apply the SRG method formulated for finite size to contract the environment tensor network. We start the evolution from a relatively large  $\tau$  and gradually reduce the value of  $\tau$  until converged. In this calculation, we reduce  $\tau$  from 0.1 to 0.01, since the ground state energy does not show significant change any more when  $\tau$  is smaller than 0.01.

After obtaining the ground-state wave function, we apply the SRG method for finite size to compute the energy, the algorithm of which has also been described in Sec. II. In this calculation, the six-fold rotational symmetry is always preserved in the coarse-graining procedure.

While the PEPS wave function itself satisfies the variational principle, the computation of the expectation value by an approximate tensor-network contraction does not necessarily satisfy the variational principle because of the approximate contraction. In fact, the norm  $\langle \Psi | \Psi \rangle$  is calculated by the contraction of a tensor network which is obtained by tracing out the physical indices in the PEPS wave function, and the approximate contraction of this tensor network is not guaranteed to be positive. As a result, the energy calculated approximately from the PEPS wave function can be lower than the exact ground-state energy. Therefore, it is necessary to assure the convergence in the computation of the expectation value under a given PEPS wave function by improving the truncation.

Figure 11 shows the convergence of the ground-state energy with increasing  $\chi$  for the Kitaev model on the 216-site lattice with the wave-function tensor dimension  $D = 6$  (upper panel) and  $D = 8$  (lower panel). Our calculation shows that the truncation error in the TRG is quite large, and the SRG can significantly reduce the truncation error. In the case of  $D = 6$ , and  $\chi = 50$ , the truncation error in the TRG is about 50%, while the truncation error in the SRG can be reduced to the order of  $10^{-3}$ . As a result, we can see that nevertheless the energy of the TRG is far away from the converged value, the SRG calculation for the finite-size lattice makes a significant improvement. While the energy computed from the TRG calculation never get converged for  $D = 6$  and  $D = 8$  with  $\chi$  up to 100, the SRG for the finite-size calculation has converged when  $\chi > 50$  for  $D = 6$  and  $\chi > 70$  for  $D = 8$ . We see that the sweeping procedure gives more significant improvement on  $D = 8$  than  $D = 6$ . That is because the truncation error increases with increasing  $D$  at a given  $\chi$ , indicating that the sweeping becomes more important in reducing the truncation error and in achieving a quicker convergence with relatively small  $\chi$  when  $D$  becomes large.

Figure 12 shows the convergence of the ground-state

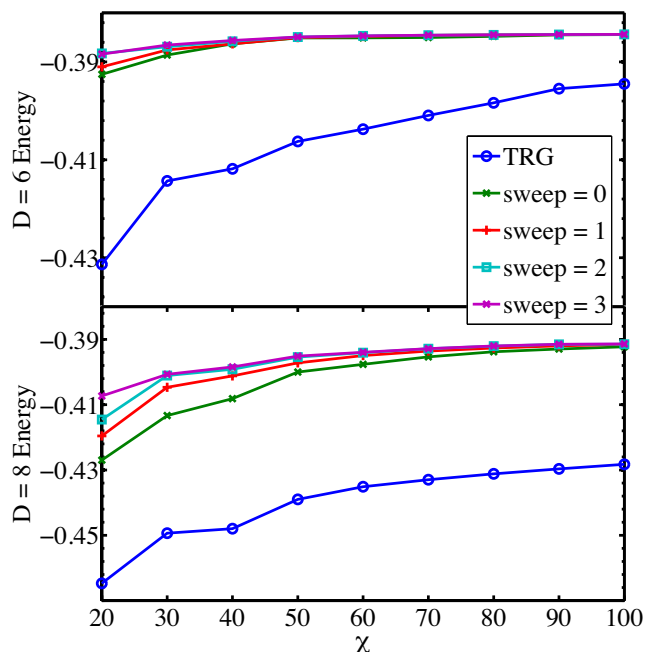


Figure 11. (color online) Ground-state energy as a function of  $\chi$  for Kitaev model on honeycomb lattice with 216 sites. The upper panel shows  $D = 6$  results and the lower panel shows the  $D = 8$  results. The TRG, finite SRG without sweeping and finite SRG with 1, 2, and 3 times sweeping results are shown in both figures. The exact energy is  $-0.393752537$ .

energy with increase of the bond dimension  $D$  on several choices of lattice size. The results are obtained by the finite SRG method with three-times sweeping. We observe that the energy error continues to decrease rapidly and unlimitedly with increasing  $D$ , indicating that the accuracy can be improved without bounds with the increase of  $D$ .

## VII. SUMMARY

In this paper, We have developed coarse-graining tensor renormalization group methods on finite periodic lattices and examined the efficiency of these methods. The TRG and HOTRG are local optimization methods which minimize the truncation error of the local tensors. In order to optimize the approximation of the whole tensor network, it is necessary to consider the effect of the environment tensor network with respect to the tensors needed to be truncated. Therefore, SRG and HOSRG methods are introduced to contract environment tensor networks and optimize the truncation of corresponding site tensors.

We have also described the algorithms and prescriptions and the way how to implement SRG and HOSRG methods to compute tensor network for finite periodic lattices. In this algorithm, differently from that for the infinite lattice, the environment tensor network is calcu-

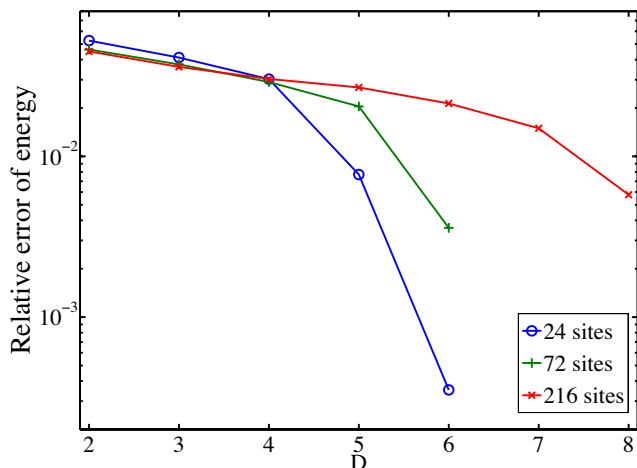


Figure 12. (color online) Relative error of ground state energy as a function of  $D$  for Kitaev model on 24, 72, and 216 sites honeycomb lattice with hexagonal shaped periodic boundary condition. Finite SRG method is applied with three-times sweeping and  $\chi$  is taken up to 100 to verify the convergence.

lated with the size of lattice at specific coarse-graining scales. When the truncation error is large, we apply the sweeping scheme to further improve the accuracy. This sweeping enables an accurate contraction of the tensor network beyond the infinite-size algorithm but with

the computational complexity similar to the corresponding infinite lattice methods. After obtaining accurate finite-size results, a reliable finite-size scaling allows to reach the thermodynamic properties, that is more accurate than that obtained from the corresponding infinite lattice method.

During the calculation, we use tensor networks with translational invariance to perform the calculation. However, it is straightforward to implement the calculation on systems without translational invariance, such as spin glass systems. The difference there is that one needs to calculate respective environment depending on every system site.

## VIII. ACKNOWLEDGMENTS

We would like to thank Sotoshi Morita for providing us a python script to calculate exact energy of finite lattice Kitaev model. The authors thank the Supercomputer Center, the Institute for Solid State Physics, the University of Tokyo for the facilities. This work was financially supported by the MEXT HPCI Strategic Programs for Innovative Research (SPIRE) and the Computational Materials Science Initiative (CMSI) under the project number hp130007 and hp140215, and the National Natural Science Foundation of China (Grants No.10934008, No.10874215, and No.11174365).

\* zhaohuihai@solis.t.u-tokyo.ac.jp

† txiang@iphy.ac.cn

‡ imada@ap.t.u-tokyo.ac.jp

<sup>1</sup> H. Niggemann, A. Klumper, and J. Zittartz, *Z. Phys. B* **104**, 103 (1997).

<sup>2</sup> T. Nishino, Y. Hieida, K. Okunishi, N. Maeshima, Y. Akutsu, and A. Gendiar, *Prog. Theor. Phys.* **105**, 409 (2001).

<sup>3</sup> F. Verstraete and J. I. Cirac, arXiv:cond-mat/0407066.

<sup>4</sup> G. Vidal, *Phys. Rev. Lett.* **99**, 220405 (2007).

<sup>5</sup> M. Levin and C. P. Nave, *Phys. Rev. Lett.* **99**, 120601 (2007).

<sup>6</sup> G. Vidal, *Phys. Rev. Lett.* **98**, 070201 (2007)

<sup>7</sup> H. C. Jiang, Z. Y. Weng, and T. Xiang, *Phys. Rev. Lett.* **101**, 090603 (2008).

<sup>8</sup> Z. C. Gu, and X. G. Wen, *Phys. Rev. B* **80**, 155131 (2009).

<sup>9</sup> Z. Y. Xie, H. C. Jiang, Q. N. Chen, Z. Y. Weng, and T. Xiang, *Phys. Rev. Lett.* **103**, 160601 (2009).

<sup>10</sup> Iztok Pirn, Ling Wang, and Frank Verstraete, *Phys. Rev. A* **83**, 052321 (2011).

<sup>11</sup> Z. Y. Xie, J. Chen, M. P. Qin, J. W. Zhu, L. P. Yang, and T. Xiang, *Phys. Rev. B* **86**, 045139 (2012).

<sup>12</sup> Z. Y. Xie, J. Chen, J. F. Yu, X. Kong, B. Normand, and T. Xiang, *Phys. Rev. X* **4**, 011025 (2014).

<sup>13</sup> G. Evenbly, and G. Vidal, arXiv:1412.0732.

<sup>14</sup> R. J. Baxter, *Exactly Solved Models in Statistical Mechanics* (Academic Press, London, 1982).

<sup>15</sup> M. Hinczewski, and A. N. Berker, *Phys. Rev. E* **77**, 011104 (2008).

<sup>16</sup> H. H. Zhao, Z. Y. Xie, Q. N. Chen, Z. C. Wei, J. W. Cai, and T. Xiang, *Phys. Rev. B* **81**, 174411 (2010).

<sup>17</sup> J. F. Yu, Z. Y. Xie, Y. Meurice, Y. Z. Liu, A. Denbleyker, H. Y. Zou, M. P. Qin, J. Chen, and T. Xiang, *Phys. Rev. E* **89**, 013308 (2014).

<sup>18</sup> A. Denbleyker, Y. Z. Liu, Y. Meurice, M. P. Qin, T. Xiang, Z. Y. Xie, J. F. Yu, and Haiyuan Zou, *Phys. Rev. D* **89**, 016008 (2014).

<sup>19</sup> I. Affleck, T. Kennedy, E. H. Lieb, and H. Tasaki, *Phys. Rev. Lett.* **59**, 799 (1987); *Commun. Math. Phys.* **115**, 477 (1988).

<sup>20</sup> G. Sierra, and M. Martin-Delgado, *Proceedings of the workshop on the Exact Renormalization Group, Faro (Portugal), 10-12 September 1998* (World Scientific, Singapore, in press).

<sup>21</sup> J. Eisert, M. Cramer, and M. B. Plenio, *Rev. Mod. Phys.* **82**, 277 (2010).

<sup>22</sup> S. Wang, Z. Y. Xie, J. Chen, B. Normand, and T. Xiang, *Chin. Phys. Lett.* **31**, 070503 (2014).

<sup>23</sup> F. Verstraete, J. I. Cirac, *Phys. Rev. Lett.* **104**, 190405 (2010).

<sup>24</sup> F. Quijandria, J. J. Garcia-Ripoll, and D. Zueco, *Phys. Rev. B* **90**, 235142 (2014).

<sup>25</sup> C. V. Kraus, N. Schuch, F. Verstraete, and J. I. Cirac, *Phys. Rev. A* **81**, 052338 (2010).

<sup>26</sup> Z. C. Gu, F. Verstraete, and X. G. Wen, arXiv:1004.2563.

<sup>27</sup> O. Sikora, H.-Wen Chang, C.-Pin Chou, F. Pollmann, and Y.-Jer Kao, *Phys. Rev. B* **91**, 165113 (2015).

<sup>28</sup> C. Krumnow, O. Legeza, and J. Eisert, arXiv:1504.00042.

- <sup>29</sup> C. Wang, S. M. Qin, and H. J. Zhou, Phys. Rev. B **90**, 174201 (2014).
- <sup>30</sup> T. Nishino, J. Phys. Soc. Jpn. **64**, 3598 (1995).
- <sup>31</sup> R. Bursill, Tao Xiang, and G. A. Gehring, J. Phys.: Cond. Matter **8**, L583 (1996).
- <sup>32</sup> X. Q. Wang, and T. Xiang, Phys. Rev. B **56**, 5061 (1997).
- <sup>33</sup> R. J. Baxter, J. Math. Phys. **9**, 650 (1968).
- <sup>34</sup> T. Nishino and K. Okunishi, J. Phys. Soc. Jpn. **65**, 891 (1996).
- <sup>35</sup> Roman Orus and Guifre Vidal, Phys. Rev. B **80**, 094403 (2009).
- <sup>36</sup> P. Corboz, J. Jordan, and G. Vidal, Phys. Rev. B **82**, 245119 (2010).
- <sup>37</sup> D. P.-Garcia, F. Verstraete, M. M. Wolf, and J. I. Cirac, Quan. Inf. Comp. **7**, 401 (2007).
- <sup>38</sup> R. Orus and G. Vidal, Phys. Rev. B **78**, 155117 (2008).
- <sup>39</sup> Z. C. Gu, M. Levin, and X. G. Wen, Phys. Rev. B **78**, 205116 (2008).
- <sup>40</sup> H. Ueda, K. Okunishi, and T. Nishino, Phys. Rev. B **89**, 075116 (2014).
- <sup>41</sup> N. Sh. Izmailian, and Chin-Kun Hu, Phys. Rev. E **65**, 036103 (2002).
- <sup>42</sup> V. Murg, F. Verstraete, and J. I. Cirac, Phys. Rev. A **75**, 033605 (2007).
- <sup>43</sup> F. Verstraete, V. Murg, and J. I. Cirac, Adv. Phys. **57**, 143 (2008).
- <sup>44</sup> J. Jordan, R. Orus, G. Vidal, F. Verstraete, and J. I. Cirac, Phys. Rev. Lett. **101**, 250602 (2008).
- <sup>45</sup> M. Lubasch, J. I. Cirac, and M-C Banuls, Phys. Rev. B **90**, 064425 (2014).
- <sup>46</sup> H. N. Phien, I. P. McCulloch, and G. Vidal, Phys. Rev. B **91**, 115137 (2015).
- <sup>47</sup> Piotr Czarnik and Jacek Dziarmaga, Phys. Rev. B **92**, 035152 (2015).
- <sup>48</sup> H. N. Phien, J. A. Bengua, H. D. Tuan, P. Corboz, and R. Orus, arXiv:1503.05345.
- <sup>49</sup> Ling Wang, Iztok Pizorn, Frank Verstraete, Phys. Rev. B **83**, 134421 (2011).
- <sup>50</sup> Yu-Kun Huang, Phys. Rev. E **83**, 036702 (2011).
- <sup>51</sup> Q. Kanfrnan, Phys. Rev. **76**, 1232 (1949).
- <sup>52</sup> A. Kitaev, Ann. Phys. (NY) **321**, 2 (2006).
- <sup>53</sup> Juan Osorio Iregui, Philippe Corboz, and Matthias Troyer, Phys. Rev. B **90**, 195102 (2014).

## Appendix A: The square lattice TRG method

In this appendix we reiterate the procedure of TRG on the square lattice, which was proposed in Ref. 5.

Here the single-sublattice tensor network is taken as an example. Every coarse-graining procedure contains two steps. The first step is to apply SVD to decompose every rank-4 site tensor

$$A_{jk,mn}^i \approx \sum_{x=1}^{\chi} U_{jk,x} \Lambda_x V_{mn,x}, \quad (\text{A1})$$

where truncation is performed and  $\chi$  largest singular values are kept.

The direction of SVD is depicted as dashed lines in Fig. 13(a). Then, 2 new tensors

$$R_x^i = U \Lambda^{\frac{1}{2}}, \quad T_x^i = V \Lambda^{\frac{1}{2}} \quad (\text{A2})$$

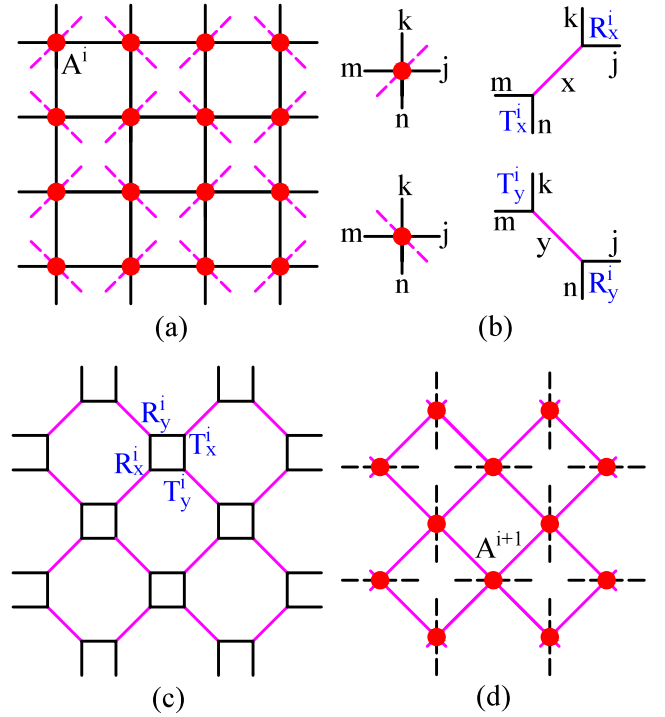


Figure 13. (color online) TRG coarse-graining scheme for square lattice tensor network<sup>5</sup>. two-sublattice tensor network is assumed. (a) Dashed lines show SVD directions. (b) SVD to decompose every rank-4 site tensor to two rank-3 tensors and keep  $\chi$  largest singular values. (c) Tensor network structure after SVD. (d) is formed from contraction of 4 tensors on every black square in (c), and the green dashed lines are the SVD directions for the next step coarse graining.

are formed as shown in the top of Fig. 13(b).  $R_y^i$  and  $T_y^i$  shown in the bottom of Fig. 13(b) are constructed similarly as  $R_x^i$  and  $T_x^i$  by Eq. (A1) and Eq. (A2) except that the SVD is applied in the perpendicular direction.

Then, the network changes the shape to Fig. 13(c), and we can contract four rank-3 tensors on every black square to form one rank-4 tensor as a coarse-grained site and then form a square-lattice tensor network, of which the size is reduced by a factor of two with the 45-degree rotated lattice configuration (Fig. 13(d)). By repeating this coarse-graining procedure, one can finally obtain a  $2 \times 2$  square-lattice tensor network, which can be contracted exactly. Then the contraction of the whole tensor network is completed.

## Appendix B: The square lattice SRG method

In this appendix, we introduce how to implement the SRG on the square lattice.

First, we do forward iteration by the TRG to contract the whole surrounding tensor network. In this iteration, the local tensors at each scale is stored. As in Fig. 14, we keep four sites on a plaquette unchanged, and coarse

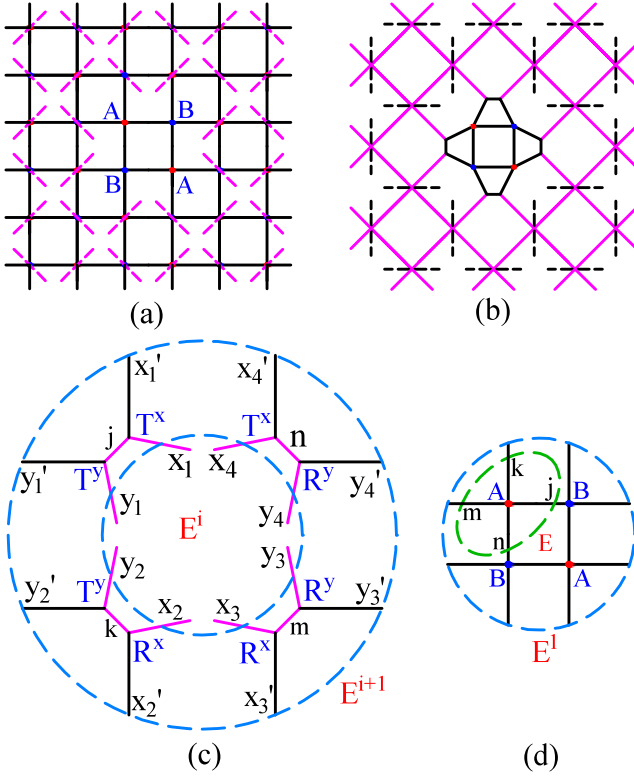


Figure 14. (color online) SRG procedure for square lattice. From (a) to (b) is one coarse-graining step for environment sites. The site tensors in the environment are decomposed along the dashed lines. (c) Relation between the neighboring scales environments  $E^i$  and  $E^{i+1}$  (dashed circles) as represented in Eq. (B1). (d) Environment tensor  $E$  of one system site tensor  $A$  is obtained by tracing out the outer part of the green ellipse.

grain the environment tensor network as shown in Fig. 14(a)(b) by the square lattice TRG. Since we assume that the environment is always infinite at every coarse-graining step of the system sites, we need to apply the coarse graining in the environment for a sufficient number of steps until converged.

Second, we do backward iteration to find the environment tensor  $E$ . Figure 14(c) schematically shows the relation between the environments of the neighboring scales, which can be represented by the following iteration formula

$$\begin{aligned}
 & E_{x_1 y_1 x_2 y_2 x_3 y_3 x_4 y_4}^i \\
 &= E_{x'_1 y'_1 x'_2 y'_2 x'_3 y'_3 x'_4 y'_4}^{i+1} T_{j x_1 x'_1}^x T_{n x_4 x'_4}^x \\
 & T_{j y_1 y'_1}^y T_{k y_2 y'_2}^y R_{k x_2 x'_2}^x R_{m x_3 x'_3}^x R_{m y_3 y'_3}^y R_{n y_4 y'_4}^y, \quad (\text{B1})
 \end{aligned}$$

where the repeated indices imply summation.

After a forward iteration, we are able to do backward iteration to contract the network by starting from tracing

out the outermost bonds and follow Fig. 14(c) to compute the environment tensor from higher to lower scales. Eventually, we can calculate the environment tensor  $E$ , which is defined as the outer part of the green ellipse in Fig. 14(d), from  $E^1$ . Note that  $E$  contains only 4 indices as  $E_{jk,mn}$ , while every  $E^i$  contains 8 indices.

After finding out the environment tensor  $E$ , SVD is applied to decompose  $E$

$$E_{jk,mn} = \sum_z X_{jk,z} \Omega_z Y_{mn,z}. \quad (\text{B2})$$

Then, we can take the environment contribution into account by constructing the following tensor

$$\tilde{A}_{z_1 z_2} = \sum_{mnjk} \Omega_{z_1}^{\frac{1}{2}} Y_{mn,z_1} A_{mn,jk} X_{jk,z_2} \Omega_{z_2}^{\frac{1}{2}}. \quad (\text{B3})$$

We compute the SVD of  $\tilde{A}$  and make truncation to keep  $\chi$  largest singular values  $\Lambda$ , the corresponding left singular vectors  $U$  and right singular vectors  $V$  as

$$\tilde{A}_{z_1 z_2} \approx \sum_{z=1}^{\chi} U_{z_1 z} \Lambda_z V_{z_2 z}. \quad (\text{B4})$$

Finally, the system site tensor  $A_{mn,jk}$  can be truncated and decomposed as a product of two tensors

$$A_{mn,jk} \approx \sum_{z=1}^{\chi} R_{mnz} T_{jkz}, \quad (\text{B5})$$

where

$$R_{mnz} = \sum_{z_1} Y_{mn,z_1} \Omega_{z_1}^{-\frac{1}{2}} U_{z_1 z} \Lambda_z^{\frac{1}{2}} \quad (\text{B6})$$

$$T_{jkz} = \sum_{z_2} X_{jk,z_2} \Omega_{z_2}^{-\frac{1}{2}} V_{z_2 z} \Lambda_z^{\frac{1}{2}}, \quad (\text{B7})$$

are two rank-3 tensors as similar as in Eq. (A2), which are on two neighboring black squares connected by a (magenta) bold bond (note that  $45^\circ$  tilted) in Fig. 13(c). Then, the network changes the shape to Fig. 13(c), and we can contract four rank-3 tensors on every black square to form one rank-4 tensor as a coarse-grained site and then repeat this coarse-graining procedure until the network can be contracted exactly. Thus the contraction of the whole tensor network can be completed.

The leading computational cost for the above method with the direct coarse graining on the square lattice is  $O(\chi^{10})$ , because the computational cost of backward iteration to contract the environment tensor  $E$ , which is shown in Fig. 14(c)(d) and Eq. (B1), scales as  $O(\chi^{10})$ .